Quality Assurance and Safety of Crops & Foods

ICC MoniQA

Quality Assurance and Safety of Crops & Foods 2010, **2**, 133–140

ORIGINAL ARTICLE

Assessment of mildew levels in wheat samples based on spectral characteristics of bulk grains

Muhammad A. Shahin, Dave W. Hatcher, Stephen J. Symons

Grain Research Laboratory, Canadian Grain Commission, Winnipeg, MB, Canada

Keywords
hyperspectral imaging; wheat; mildew.

Correspondence:
Muhammad A. Shahin, Grain Research Laboratory, Canadian Grain Commission, 1404-303 Main Street, Winnipeg, MB, Canada R3C 3G8.
Email: muhammad.shahin@grainscanada.gc.ca

GRL # 1033

Received 23 November 2009; revised 12 April 2010; accepted 29 May 2010.

doi:10.1111/j.1757-837X.2010.00070.x

Abstract

Background Mildew damage is a quality defect that has an adverse effect on the quality of flour. *Aims* The objective of this study was to develop a rapid and consistent imaging method to quantify the extent of mildew damage in wheat samples. *Materials and methods* A hyperspectral imaging system with a wavelength range of 400–1000 nm was used to detect and quantify mildew in 65 Canada Eastern Soft Red Winter (CESRW) wheat samples. Partial least square (PLS) regression calibrations were developed to predict mildew levels based on the spectral characteristics of the bulk samples. *Results and discussion* Predictions from a model with 4 PLS factors based on image standard deviation spectra matched well with the visual assessment of the samples with an R^2 approaching 0.87 and an RMSE of 0.76 on the validation set. Accuracy of the PLS classification for 9 mildew levels was 90.6% (± 1 level) and 84.4% for 3 inspector grades. *Conclusion* This study confirms that potential use of hyperspectral imaging for mildew detection in commercial operations is possible.

Shahin MA, Hatcher, DW, Symons JS (2010). Assessment of mildew levels in wheat samples based on spectral characteristics of bulk grains. *Quality Assurance and Safety of Crops & Foods*, **2**, 133–140.

Introduction

Mildew damage is a serious quality defect that has a negative impact on processing quality and commercial value of wheat (Dexter & Edwards, 1998). Mildew is a fungal contamination caused by adverse growing conditions that imparts a grey discoloration initially on the brush end of the kernel, which begins to encompass the entire kernel as damage increases. It is caused by various fungi such as Cladosporium and Alternaria alternata that thrive under wet humid conditions. The mildew damage is more noticeable when harvest is delayed under wet conditions (http://www.omafra.gov.on.ca/english/crops/field/news/croppest/2008/12cpo08a6.htm). Review of the scientific literature indicated that research has been primarily focused on wheat breeding programs to impart resistance to mildew as resistance is believed to be derived by the 1AL.1RS wheat-rye chromosome translocation (Graybosch *et al.*, 1999; Yoshida *et al.*, 2001; Li *et al.*, 2007) as observed in Triticale (Svoboda *et al.*, 1991). Wheat milling performance decreases with increasing levels of mildewed kernels of common wheat (Everts *et al.*, 2001) but no impact on semolina yield was reported (Dexter & Matsuo, 1982). The Canadian Grain Commission (CGC) is the Canadian federal agency responsible for establishing tolerances for the various grades of wheat classes grown in Canada and has carried out extensive research to ensure that the level of mildewed kernels within each grade are appropriate and reflect the intrinsic value of the grain. Internal reports (unpublished) indicate that Canada Eastern White wheat displayed a significant shift in the resulting flour colour, decreased flour yield straight grade flour from -1.6 Kent Jones (KJ) units for a No. 1 grade to -0.3 KJ units for a No. 3 grade. The impact of mildew on durum wheat products is primarily a significant increase (2–3-fold) in the speckiness of the resulting spaghetti (Dexter & Matsuo, 1982). Current grading systems are based on a relatively slow and subjective human visual inspection by trained inspectors, whereby the degree of damage to kernels is assessed by comparison with standard samples or

mildew-guides to give an overall subjective visual assessment of severity of damage. However, it remains difficult to quantify the amount of mildew damage through visual inspection, especially for samples with light to moderate degrees of damage. It is important to determine the extent of damage as the severity of damage is inversely related to the quality of flour and bread produced from mildewed wheat. Fast and accurate objective methods are required to facilitate segregation and cope with high volume inspection demanded by the grain industry to meet the needs of national as well as international trade.

Luo *et al.* (1999) used conventional image analysis to detect mildew and five other types of damage factors (broken, grass-green/green-frosted, black-point/smudge, heated, and bin/fire-burnt) on CWRS wheat kernels. They were able to detect visually obvious severely damaged mildewed kernels highly accurately (97%), however, detection of visually challenging slight or moderate levels of mildew damage was not attempted. The identification of damaged regions of individual kernels by imaging appears to be a logical solution; however, variations in the discoloration of the damaged regions and the colour of underlying kernels make this impossible to achieve using a traditional imaging platform. Hyperspectral imaging (HSI) can provide a workable solution in this situation. HSI is a combination of conventional imaging and spectroscopy that can provide information with high spatial and spectral resolution. Hyperspectral images commonly known as hypercubes are three-dimensional data structures containing both the spatial and spectral information. Each pixel in a hypercube contains the entire spectrum that can be used as a fingerprint to characterize the composition of that particular pixel.

HSI systems have been used in a wide variety of fields including remote sensing, pharmaceutical, medical, and agricultural industries. Recently, this technology has emerged as a research tool for food quality and safety control (Gowen *et al.*, 2007). In the agro-food industry, HSI applications have been reported for quality assessment of fruits (Kim *et al.*, 2002; Lu, 2003), vegetables (Cheng *et al.*, 2004; Gowen *et al.*, 2008), poultry (Park *et al.*, 2002), beef steaks (Naganathan *et al.*, 2008), and cereal grains (Cogdill *et al.*, 2004; Goretta *et al.*, 2006; Lin *et al.*, 2006; Shahin & Symons, 2008). Recent studies have shown that HSI could distinguish sprout damaged (Singh *et al.*, 2009; Xing *et al.*, 2009) as well as stained and fungal infected (Berman *et al.*, 2007; Singh *et al.*, 2007) wheat kernels from sound kernels. Spectral characteristics of mildewed wheat kernels have been reported to be significantly different from those of sound undamaged kernels (Shahin & Symons, 2007). These spectral differences can be utilized to determine the extent of mildew damage in wheat samples. The objective of this study was to develop, using real world commercial samples, a rapid and consistent HSI method to quantify the extent of mildew damage in wheat samples which is highly correlated to existing inspector visual assessments. This is the first step in the development of a systematic approach to creating objective measurements for grain quality assurance. Quantification of the effect of other grading factors on grain quality can be determined by separate studies as we can only approach this work in discrete and manageable steps.

Materials and methods

Samples

Sixty-five samples of Canada Eastern Soft Red Winter (CESRW) class of wheat from the 2008-crop year were collected from a diverse series of sites throughout southern Ontario. In the Canadian grading system, a class of wheat refers to a collection of varieties with common visual and functional characteristics. The sample set comprised of 25R47, Becher, Emmitt, Huntley, and Vienna varieties registered under the CESRW class of wheat (http://www.grainscanada.gc.ca/legislation-legislation/orders-arretes/2009/2009-19-eng.htm). These totally independent samples represented significant variations in growing conditions and soil types. Each sample was in excess of 1 kg and was graded by trained inspectors from the Industry Services division of the CGC. The commercial samples chosen for this study characterized the maximum range of mildew damage kernels found in eastern Canada and were representative of the normally assigned three CGC grades (1–3). Based on the severity of mildew damage, as determined by the inspectors examining damaged kernels with a 10 magnification Lupe, the samples were further assigned to one of nine levels (three levels within each grade) namely high1 (H1), medium1 (M1), low1 (L1), . . . , and low3 (L3) representing the top of grade 1, the middle of grade 1, bottom of grade 1, . . ., and bottom of grade 3, respectively (Table 1). For data analyses

Table 1 Inspector visual grades and grade level scores of samples based on mildew damage

Grades	Grade level	Numerical scale	Description
1 CE SRW	H1	1	Top of grade 1
	M1	2	Middle of grade 1
	L1	3	Bottom of grade 1
2 CE SRW	H2	4	Top of grade 2
	M2	5	Middle of grade 2
	L2	6	Bottom of grade 2
3 CE SRW	H3	7	Top of grade 3
	M3	8	Middle of grade 3
	L3	9	Bottom of grade 3

and model building, the inspector scores were converted to a numerical scale from 1 to 9 where a score of 1 corresponded to high quality No. 1, 2 corresponded to moderate mildew level within the No. 1 grade, while 3 corresponded to the lowest acceptable No. 1 grade. Assignment of 4 through 6 corresponded to the different levels within the No. 2 grade, while 7 through 9 represented the variations found within the No. 3 grade. The samples were scanned and analysed for mildew damage with a push-broom type HSI system in the 400–1000 nm wavelength range (VNIR 100E Lextel Intelligence Systems, Jackson, MS, USA) as described next.

HSI system

The imaging system consisted of a prism-grating-prism spectrograph, a high-resolution 14-bit CCD camera (PCO Imaging, Germany), a C-mount focusing lens, a motor for lens motion control, and a personal computer. The motorized lens assembly moved in front of the camera allowing for imaging stationary targets. The system came equipped with the image capture software HyperVisual that could scan up to 800 lines of 1600 pixels per line with 1200 spectra per pixel between 260 and 1084 nm. This translates to a spectral resolution of 0.69 nm. The nominal spectral range of the spectrograph (ImSpector V10E, Specim, Oulu, Finland) used was 400–1000 nm – spectra outside this range is nothing but noise, hence it must be discarded. The HyperVisual software allowed for a spatial binning of two and a spectral binning of two, four and eight. Wavelength calibration of the system was performed using Mercury-Argon (M-6035; Newport Oriel, Stratford, CT, USA) and Krypton (M-6031; Newport Oriel) pencil lights. The system was enclosed in a light-tight cabin to reduce the effect of stray ambient light as shown in Figure 1. Two 250 W quartz–tungsten–halogen lamps were used for sample illumination. Power to each lamp was regulated through a radiometric power supply (M-69931; Newport Oriel). The lamps were enclosed in two lamp housings with cooling fans (M-66881; Newport Oriel). The lamp housings were kept outside the cabin to minimize heat load inside the cabin. Collimated light beams from lamp housings were deflected with two 10×10 cm aluminium coated mirrors (NT45-343; Edmund Optics, Barrington, NJ, USA) to illuminate the sample from two sides. This lighting arrangement minimized the shadowing effect of three-dimensional objects (wheat grains, in this case).

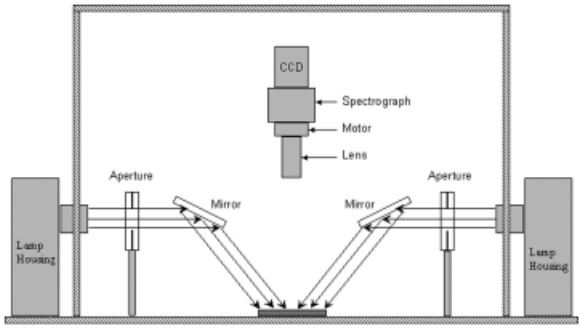

Figure 1 Schematic of the hyperspectral imaging camera system and lighting arrangement.

Image acquisition and calibration

For image capture, a $16 \times 8 \times 1$ cm wooden tray filled with approximately 200 g of wheat representative of a 1 kg sample was placed directly under the camera and an 800×400 spatial $\times$ 300 spectral hypercube was collected for each sample. The 200 g of wheat grains per sample adequately covered the wooden tray with little visibility of the backing as shown in Figure 2a. Spatial binning of two and spectral binning of four were used while the exposure time was set at 60 ms.

Dark current and white light reference responses were collected before imaging each sample to calibrate spectra at each pixel in terms of percent reflectance value. A polytetrefluoroethylene panel with 99% reflectance (Spectralon, Labsphere, USA) was used to collect white light reference images. Dark current response images were collected with

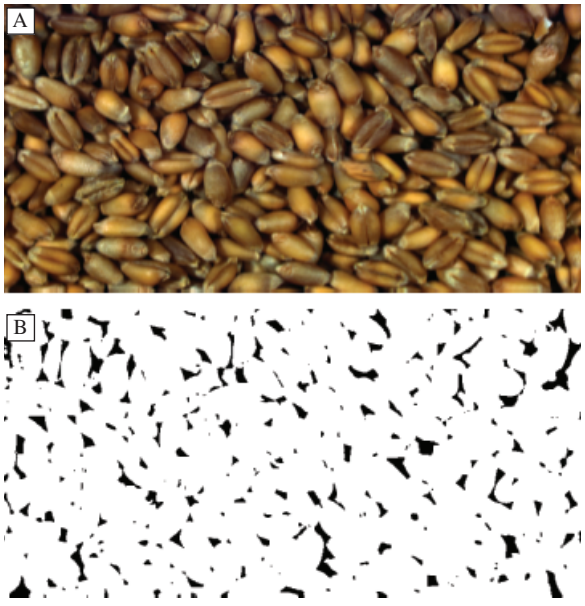

Figure 2 (A) True colour (RGB) representation of hyperspectral image of a CESRW wheat sample; (B) region of interest or mask image.

the lamp off and a cap covering the focusing lens. Calibrated reflectance images (R) were calculated using:

$$R = \frac{I_{raw} - I_{dark}}{I_{white} - I_{dark}} \quad (1)$$

where I_{raw} is the non-calibrated original image of a sample, I_{white} is the image of the white reference and I_{dark} is the dark current image. Calibrated hypercubes were subset to keep 218 bands between 400 and 1000 nm for further analyses.

Spectral data extraction and analyses

It would be ideal to classify each pixel in the hyperspectral image based on spectral signatures, however, true classification of each pixel were not known for validation. In fact, only one inspector score for the entire image (sample) was available for comparison. In order to mimic the current human visual inspection, the image mean intensity and spatial variability in the image plane were investigated for their ability to segregate samples according to the extent of mildew damage as assessed through visual inspection. To achieve this, image mean and standard deviation values were computed at each wavelength in the hypercube of a sample to generate what was called as the image mean spectrum and image standard deviation spectrum, respectively. Darker areas in the image (voids) were excluded from calculations to minimize the effect of shadows or 'holes' in the image plane. The entire image (800 × 400 pixel) minus the voids was used as the region of interest (ROI) for calculating image mean and standard deviation spectra. A mask or the ROI image was created from an image band at 850 nm using a dynamic threshold value based on image statistics to accomplish this as shown in Figure 2b. It might appear that most of the power of the imaging has been thrown away with the spatial averaging procedure, the two spectra from a sample were expected to contain information on proportions of mildewed and non-mildewed (sound) kernels in that particular sample as the spectral response of mildewed and sound kernels have been shown earlier to differ significantly (Shahin & Symons, 2007). The standard deviation spectrum particularly was thought to reflect spatial variability in a sample as a measure of mildew damage. A macro written in IDL software (Version 7.0.2; ITT Visual Information Solutions, Denver, CO, USA) was used to extract image mean and standard deviation spectra for all the samples in a batch mode.

Mildew level predictions

The image mean spectra were peak normalized by dividing each spectrum with its value at 950 nm, which corresponds to a water band, in order to minimize the effects of moisture variations among samples and lighting inconsistency within the image plane. Normalized image mean spectra and the standard deviation spectra, separately as well as in combination, were used as input variables to develop partial least squares (PLS) regression models to predict visually assessed mildew levels using the Unscrambler software (version 9.8, CAMO Software, Oslo, Norway). For regression models development, the sample set was randomly split into two subsets. The calibration subset consisting of 33 samples was used to develop PLS models while validation subset consisting of 32 samples was used for performance evaluation of the models. The same samples were kept in the two sample sets to compare different models. Performance of PLS models was evaluated based on coefficient of determination (R^2) and root mean squared error (RMSE) as the performance criteria. In addition, the model performance was validated on mildew guides or reference samples (4) prepared by the Inspection Division (CGC) for 2008 and 2009 crop years. For mildew level classification, output of the best PLS model was partitioned into nine equally spaced discrete classes using the following rule base:

if (output $<$ 1.5) then class = high1
if (1.5 $\geq$ output $<$ 2.5) then class = medium1
if (2.5 $\geq$ output $<$ 3.5) then class = low1
if (3.5 $\geq$ output $<$ 4.5) then class = high2
if (4.5 $\geq$ output $<$ 5.5) then class = medium2
if (5.5 $\geq$ output $<$ 6.5) then class = low2
if (6.5 $\geq$ output $<$ 7.5) then class = high3
if (7.5 $\geq$ output $<$ 8.5) then class = medium3
if (output $\geq$ 8.5) then class = low3

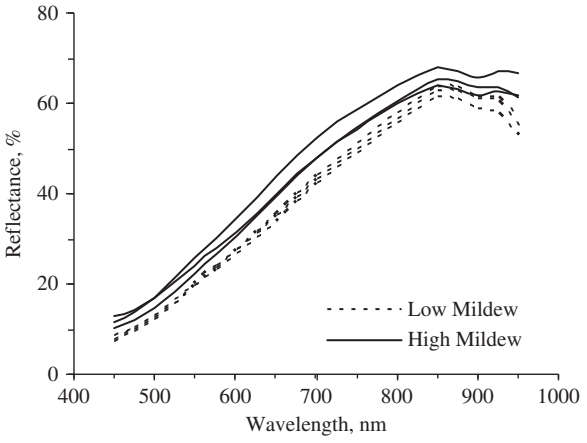

Figure 3 Image mean spectra for samples with different levels of mildew damage.

Results and discussion

Spectral characteristics of bulk grains

Figure 3 shows the image mean spectra for a number of CESRW samples with low and high levels of mildew damage. The mean spectra tended to separate the samples into two groups between 600 and 800 nm range. However, the separation was not ideal. The image standard deviation spectra for the same set of samples, on the other hand, separated the two groups quite nicely (Figure 4). The separation was obvious at wavelengths around 450 nm and higher than 700 nm. These observations suggested that the image standard deviation spectra could potentially distinguish among samples with different levels of mildew better than the image mean spectra. The image mean spectra within 600–850 nm might provide some additional information that could improve the overall segregation.

PLS regression

A number of PLS regression models were investigated for predicting mildew levels in CESRW wheat based on different spectra as input to the models. Performance of these models on the calibration as well as validation sets is summarized in Table 2. A model with 6 PLS factors based on image mean spectra predicted the inspectors scores for 9 mildew levels with an R^2 of 0.81 and RMSE of 0.89 on the validation set. The entire spectrum (450–950 nm) contributed significantly in this model, however, wavelengths in the blue (450–500 nm) and the NIR (870–930 nm) regions showed more predominant effect as shown by the regression coefficients plot (Figure 5a). The model based on image standard deviation spectra performed better than the one based on image mean spectra as the model input in terms of fewer PLS factors, higher R^2 and lower RMSE, especially for the validation set. A model with four factors predicted the nine mildew levels with an R^2 of 0.86 and RMSE of 0.77. The regression coefficients (Figure 5b) showed fewer peaks and valleys in this case indicating predominant wavelengths linked to colour changes in the blue–green region (450–560 nm) and some structural changes detected in the higher end of the spectrum (800–950 nm). Combining the image mean and image standard deviation spectra slightly improved the model performance with an R^2 of 0.865 and RMSE of 0.76 on the validation set. R^2 and RMSE on the calibration set were of 0.869 and 0.75, respectively. The regression coefficients for this model were dominated by the image standard deviation spectra with little contribution from the image mean spectra (Figure 5c). Based on these results, either of the last two models could be used to predict and quantify the extent of mildew damage on a scale from 1 to 9 where a smaller value meant a lower mildew damage and vice a versa. However, the model based on the standard deviation spectra alone seemed a better option because of its comparable performance with less computational requirements.

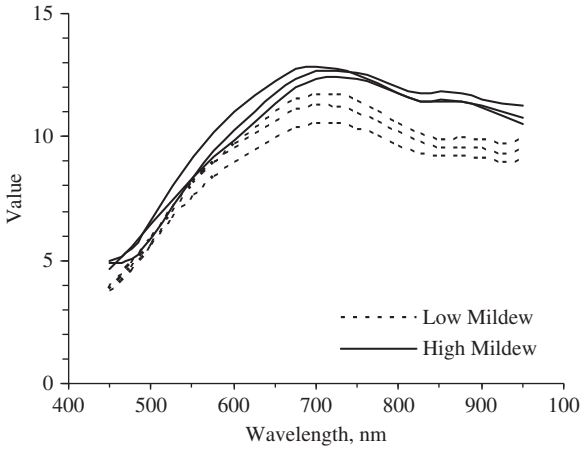

Figure 4 Image standard deviation spectra for samples with different levels of mildew damage.

Mildew level classification

To be consistent with the current grading system, the output from the best PLS model was partitioned into nine classes corresponding to nine mildew levels assessed by the grain inspectors. Classification results for the validation set are presented in Table 3. The mildew levels in 20 of the 32 CESRW samples the validation set were correctly predicted achieving an accuracy of 62.5% within the nine levels of

Table 2 Partial least square (PLS) regression results

PLS model input data	Number of PLS factors	Calibration		Validation	
		R^2	RMSE	R^2	RMSE
Image mean spectra	6	0.860	0.77	0.815	0.89
Image standard deviation spectra	4	0.866	0.75	0.861	0.77
Combined image mean and standard deviation spectra	4	0.869	0.75	0.865	0.76

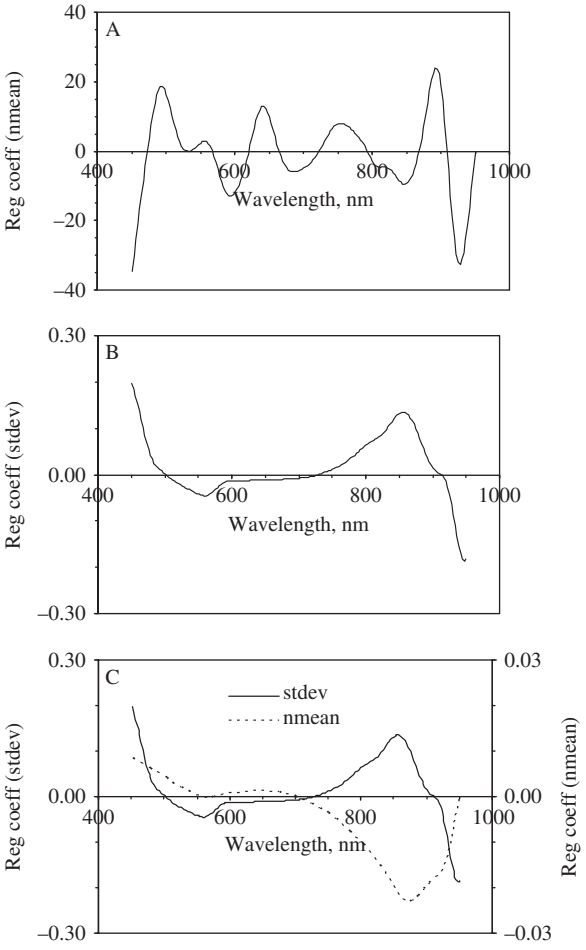

Figure 5 Regression coefficients (Reg coeff) for PLS models developed with (A) normalized image mean spectra, (B) image standard deviation spectra, and (C) normalized image mean (nmean) and standard deviation (stdev) spectra combined.

classification. Accuracy for the calibration set was 66.67% (22 out of 33). Most of the misclassifications, however, were to the adjacent mildew levels, e.g., a sample with an inspector assessed mildew level of high3 (H3) was misclassified as either low2 (L2) or medium3 (M3). Accuracy of classification within ± 1 mildew level approached 90.62% (29/32) for the validation set and 96.97% (32/33) for the calibration set. Accuracy of classification for the same grade as the inspector's grade was 84.37% (27/32) on the validation set and 84.85% (28/33) on the calibration set.

When tested on the four mildew guides or reference samples for two consecutive crop years, the model correctly predicted the mildew damage within ± 1 level. This demonstrated the robustness of the model to certain extent. While numerically this may not seem significant, the simple fact that the standard samples are used as the reference to grade millions of tonnes of wheat exported from Canada validates our approach and modelling of mildew damage in a commercial inspection environment.

The proposed method offers a number of advantages over the previous studies. Firstly, it deals with a range of mildew levels (light to moderate to severe) over three grades as opposed to the conventional imaging method reported by Luo *et al.*, (1999), which handled only visually obvious severely mildewed kernels. Secondly, the current method evaluates bulk samples requiring no sample preparations making sample presentation and image acquisition much easier and faster than for single-kernel evaluations done previously (Berman *et al.*, 2007; Singh *et al.*, 2007). Thirdly, the proposed method is based on the measurements in the visible-NIR spectral range (400–1000 nm), which offers a far

Table 3 Partial least square (PLS) classification of CE SRW samples in the validation set into nine mildew levels

Grades	Grade level	Predicted into mildew grade level									Total actual
		H1[1]	M1	L1	H2	M2	L2	H3	M3	L3	
1 CE SRW	H1	–	–	–	–	–	–	–	–	–	–
	M1	0	**2**	0	0	0	0	0	0	0	2
	L1	0	0	**1**	0	0	0	0	0	0	1
2 CE SRW	H2	0	0	0	**3**	2	0	0	0	0	5
	M2	0	0	0	0	**4**	1	0	0	0	5
	L2	0	0	0	0	0	**3**	2	0	0	5
3 CE SRW	H3	0	0	0	0	0	2	**2**	1	0	5
	M3	0	0	0	0	0	1	0	**3**	0	4
	L3	0	0	0	0	0	0	2	1	**2**	5
Total predicted		0	2	1	3	6	7	6	5	2	32
		Grade 1CE SRW				Grade 2CE SRW			Grade 3CE SRW		

Numbers in bold indicate correctly classified number of samples. Shaded rows indicate classification within ± 1 mildew level (validation set).
[1]H, M and L stand for high, medium and low, respectively.

less expensive solution compared with the SWIR systems (1000–2500 nm) used in previous studies (Berman *et al*., 2007; Singh *et al*., 2007).

Conclusions

The results of this study have shown that HSI in the visible-NIR wavelength range offers the ability to detect and discern varying degrees of severity of mildew damage in commercial CESRW wheat samples. Using PLS regressions, mildew levels (1–9) can be predicted with an accuracy approaching 91% (± 1 level). Comparison with the existing subjective visual assessment with trained inspectors, predicted wheat grade (1–3) based on mildew alone achieved an accuracy exceeding 84%. This confirms that potential use of HSI for mildew detection in commercial operations is possible.

Acknowledgements

The authors thank the Inspection Division of the CGC for providing inspected samples for this research. They would also like to thank Loni Powell of the Image Analysis & Spectroscopy (CGC) for scanning the samples.

Contribution: Muhammad A. Shahin, deigned and performed research, collected and analyzed data, wrote the paper.

Contribution: Dave W. Hatcher, helped in experimental design, interpretation of results.

Contribution: Stephen J. Symons, overall research management, reviewed the paper.

References

Berman M., Connor P.M., Whitbourn L.B., Coward D.A., Osborne B.G., Southan M.D. (2007) Classification of sound and stained wheat grains using visible and near infrared hyperspectral image analysis. *Journal of Near Infrared Spectroscopy*, **15**, 351–358.

Cheng X., Chen Y.R., Tao Y., Wang C.Y., Kim M.S., Lefcourt A.M. (2004) A novel integrated PCA and FLD method on hyperspectral image feature extraction for cucumber chilling inspection. *Transactions of the ASAE*, **47**, 1313–1320.

Cogdill R.P., Hurdburgh C.R., Rippke G.R. (2004) Single kernel maize analysis by near-infrared hyperspectral imaging. *Transactions of the ASAE*, **47**, 311–320.

Dexter J.E., Edwards N.M. (1998) The implications of frequently encountered grading factors on the processing quality of common wheat. Association of Operative Millers, Bulletin, 7115.

Dexter J.E., Matsuo R.R. (1982) Effect of smudge and blackpoint, mildewed kernels, and ergot on durum wheat quality. *Cereal Chemistry*, **59**, 63–69.

Everts K.L., Leath S., Finney P.L. (2001) Impact of powdery mildew and leaf rust on milling and baking quality of soft red winter wheat. *Plant Disease*, **85**, 423–429.

Goretta N., Roger J.M., Aubert M., Bellon-Maurel V., Campan F., Roumet P. (2006) Determining vitreouness of durum wheat kernels using near infrared hyperspectral imaging. *Journal of Near Infrared Spectroscopy*, **14**, 231–239.

Gowen A.A., O'Donnell C.P., Cullen P.J., Downy G., Frias J.M. (2007) Hyperspectral imaging – an emerging process analytical tool for food quality and safety. *Trends in Food Science and Technology*, **18**, 590–598.

Gowen A.A., O'Donnell C.P., Taghizadeh M., Gaston E., O'Gorman A., Cullen P.J., Frias J.M., Esquerre C., Downey G. (2008) Hyperspectral imaging for the investigation of quality deterioration in sliced mushrooms (*Agaricus bisporus*) during storage. *Sensing and Instrumentation for Food Quality and Safety*, **2**, 133–143.

Graybosch R.A., Lee J.H., Peterson C.J., Porter D.R., Chung O.K. (1999) Genetic, agronomic and quality comparisons of two 1AL.1RS. wheat-rye chromosal translocations. *Plant Breeding*, **118**, 125–130.

Kim M.S., Lefcourt A.M., Chao K., Chen Y.R., Kim I., Chan D.E. (2002) Multispectral detection of fecal contamination on apples based on hyperspectral imagery. *Transactions of the ASAE*, **45**, 2027–2037.

Li G., Chen P., Zhang S., Wang X., He Z., Zhang Y., Zhao H., Huang H., Zhou X. (2007) Effects of the 6VS.6AL translocation on agronomic traits and dough properties of wheat. *Euphytica*, **155**, 305–313.

Lin L.H., Lu F.M., Chang Y.C. (2006) Development of a near-infrared imaging system for determination of rice moisture. *Cereal Chemistry*, **83**, 498–504.

Lu R. (2003) Detection of bruise on apples using near-infrared hyperspectral imaging. *Transactions of the ASAE*, **46**, 523–530.

Luo X., Jayas D.S., Symons S.J. (1999) Comparison of statistical and neural network methods for classifying cereal grains using machine vision. *Transactions of the ASAE*, **42**, 413–419.

Naganathan G.K., Grimes L.M., Subbiah J., Calkins C.R., Samal A., Meyer G.E. (2008) Partial least squares analysis of near-infrared hyperspectral images for beef tenderness prediction. *Sensing and Instrumentation for Food Quality and Safety*, **2**, 178–188.

Park B., Lawrence K.C., Windham W.R., Buhr R.J. (2002) Hyperspectral imaging for detecting fecal and ingesta contaminants on poultry carcasses. *Transactions of the ASAE*, **45**, 2017–2026.

Shahin M.A., Symons S.J. (2007) The use of hyperspectral imaging to characterize wheat grading factors. *Proceedings of the 13th International Conference on NIR*, Umea, Sweden.

Shahin M.A., Symons S.J. (2008) Detection of hard vitreous and starchy kernels in amber durum wheat samples using hyperspectral imaging. *NIR News*, **19**, 16–18.

Singh C.B., Jayas D.S., Paliwal J., White N.D.G. (2007) Fungal detection in wheat using near-infrared hyperspectral imaging. *Transactions of the ASABE*, **50**, 2171–2176.

Singh C.B., Jayas D.S., Paliwal J., White N.D.G. (2009) Detection of sprouted and midge-damaged wheat kernels using near-infrared hyperspectral imaging. *Cereal Chemistry*, **86**, 256–260.

Svoboda L.H., Mora M.J., Matzenbacher R.G. (1991) Technological quality and agronomic performance of triticale cultivars in Brazil. *In Proceedings of the International Triticale Symposium*. Passo Fundo, Brazil, pp. 460–465.

Xing J., Hung P., Symons S., Shahin M., Hatcher D. (2009) Using a SWIR hyperspectral imaging system to predict alpha amylase activity in individual Canadian Western wheat kernels. *Sensing and Instrumentation for Food Quality and Safety*, **3**, 211–218.

Yoshida H., Otobe K.C., Yanagisawa T., Yamaguchi I., Seko H., Ushiyama T., Amano Y., Miyakawa S., Kuroda A. (2001) Breeding of a new wheat (Triticum aestivum) cultivar Ayahikari with good noodle making quality. *Bulletin National Agriculture Research Center (Japan)*, **34**, 17–35.